

Liquid phase hydrogen peroxide decomposition for micro-propulsion applications

M. Ryan McDevitt^a and Darren L. Hitt^{*}

Department of Mechanical Engineering, University of Vermont, Burlington, Vermont, USA

(Received February 26, 2016, Revised April 16, 2016, Accepted April 21, 2016)

Abstract. Hydrogen peroxide is being considered as a monopropellant in micropropulsion systems for the next generation of miniaturized satellites ('nanosats') due to its high energy density, modest specific impulse and green characteristics. Efforts at the University of Vermont have focused on the development of a MEMS-based microthruster that uses a novel slug flow monopropellant injection scheme to generate thrust and impulse-bits commensurate with the intended micropropulsion application. The present study is a computational effort to investigate the initial decomposition of the monopropellant as it enters the catalytic chamber, and to compare the impact of the monopropellant injection scheme on decomposition performance. Two-dimensional numerical studies of the monopropellant in microchannel geometries have been developed and used to characterize the performance of the monopropellant before vaporization occurs. The results of these studies show that monopropellant in the lamellar flow regime, which lacks a non-diffusive mixing mechanism, does not decompose at a rate that is suitable for the microthruster dimensions. In contrast, monopropellant in the slug flow regime decomposes 57% faster than lamellar flow for a given length, indicating that the monopropellant injection scheme has potential benefits for the performance of the microthruster.

Keywords: micropropulsion; heterogeneous catalysis; micro-reactor; hydrogen peroxide

1. Introduction

Next generation small satellites, also known as nanosats, have masses significantly lower than standard satellites, often in the range of 1 to 10 kg. These satellites are being developed for numerous applications related to research, defense and industry. An important subcategory of nanosats are those built on the CubeSat specification, which allows for cube shaped satellites, as small as 10 cm per side, with masses as low as 1.33 kg. CubeSats offer a low cost alternative to traditional satellites due to their low Size, Weight and Power (SWaP). Recent advances in fields such as additive manufacturing, microfluidics, MicroElectroMechanical Systems (MEMS), low power microelectronics, high efficiency solar cells, and advanced materials all contribute to the continued development of on-board propulsion systems for the CubeSat platform. Future CubeSats, incorporating these advances, could enable scientific missions that would be impossible or financially imprudent using traditional satellites.

^{*}Corresponding author, Professor, E-mail: darren.hitt@uvm.edu

^aPh.D., E-mail: ryan.mcdevitt@uvm.edu

There are many potential advantages of incorporating propulsion systems on future CubeSat missions. Some of these advantages include, extended mission lifetime, maneuvering ability, formation flying, proximity operations, fine attitude control, drag make-up, and de-orbiting (NASA Mission Design Staff 2014). Today, NASA's CubeSat Launch Initiative (CSLI) plans on providing low cost access to space for research purposes for over 100 CubeSats developed by both the United States government as well as non-profit organizations. Without on-board propulsion systems, these missions are expected to have a lifespan of approximately 90 days before they fall to earth and burn up in the atmosphere. Through the integration of propulsion systems, lifetimes on missions similar to those of the CSLI missions could be greatly extended providing the government and independent researchers the ability to collect significantly more data.

There are many types of CubeSat propulsion systems in development, such as solar sails, electrodynamic tethers, ion electrospray, miniaturized Hall thrusters, solid rocket motors, liquid chemical thrusters, cold gas thrusters, and pulsed plasma thrusters (Mueller, *et al.*, 2010). While many of these technologies offer great promise, the high cost of manufacturing these systems along with the need for advancements in electric power generation and storage, thermal management, and power processing unit (PPU) technologies currently hinder the implementation of these propulsion systems on CubeSats. A reliable, low-cost, easily manufactured propulsion system is necessary for CubeSat propulsion to be widely implemented.

One promising technology is the miniaturization of monopropellant thrusters based on rocket grade hydrogen peroxide (HTP) or hydrazine (Gauer, Telitschkin *et al.* 2014, Huh and Kwon 2014, Krejci, Woschnak *et al.* 2013, Valenzuela, Garcia *et al.* 2011). Hydrogen peroxide is a desirable monopropellant due to its modest specific impulse ($I_{sp}=150$ s), high storage density (1450 kg/m³) and its "green" characteristics (Whitehead 1998). Hydrogen peroxide decomposition is a highly exothermic reaction, with adiabatic flame temperature of HTP listed between 886° - 1251° K depending on concentration, but the activation energy of this reaction is high enough to prevent spontaneous reaction in properly designed storage. When exposed to a catalyst, which may include silver, platinum, various iron compounds or a range of other metals, the activation energy is lowered sufficiently to allow the reaction to proceed at room temperature.

The aerospace community has a long history with HTP-based rockets, so it is a natural choice when investigating the development of micro-scale thrusters. Cervone, Torre *et al.* (2006) developed a small-scale thruster with thrust levels of ≈ 5 N using silver gauss and pellets as a catalyst. Attempts to shrink this design to smaller scales ($O[500$ μ m]) were unsuccessful due to pressure drop issues associated with the packed bed. A microscale thruster, developed at NASA Goddard Space Flight Center (GSFC) used MEMS-manufacturing techniques to develop a thruster capable of meeting design requirements recommended by Thomas (2000) including a thrust level of 500 μ N, impulse bit of 1 - 100 μ Ns and a specific impulse of 160 s. The schematics for that prototype, and an image of a fabricated prototype are shown in Fig. 1. That thruster included a catalytic chamber with an array of square silver-coated pillars oriented at 45° to the flow (Hitt, Zakrzewski *et al.* 2001). While this system was an effective demonstration of a microscale monopropellant microthruster, it suffered from performance degradation as the silver coating flaked off the pillars at high temperatures.

A new monopropellant microthruster has been proposed at the University of Vermont, which serves to build upon the GSFC system to offer improved performance. This proposed microthruster has been divided into 3 subsystems for study, as shown in Fig. 2. The first subsystem is a fuel delivery system that provides discrete slugs of fuel to the catalytic chamber, which has been reported on by McDevitt and Hitt (2009). The second subsystem is the catalytic chamber that

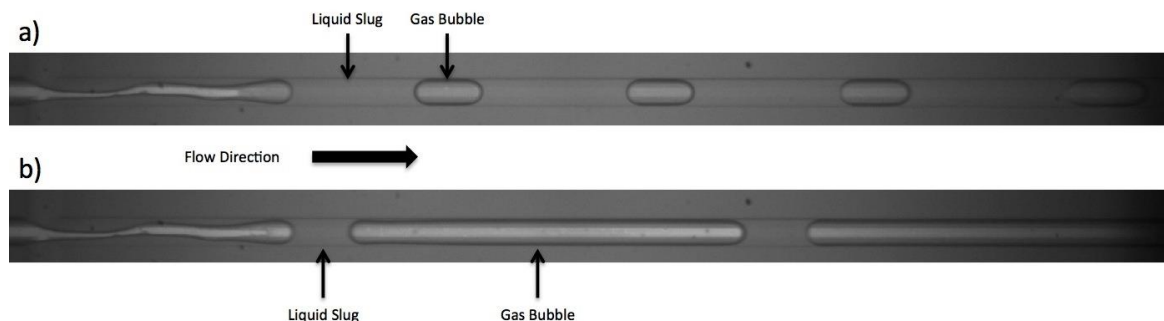


Fig. 3 Images of slug formation in a 50 μm microchannel. The inlet pressures in (a) are all set at 206 kPa. In (b) the liquid inlet pressure is set at 206 kPa and the air inlet pressure is set at 211 kPa resulting in very different slug characteristics

process that begins once all of the reactants and products are in a gaseous state. This model has provided valuable information about the effects of thermal and mass diffusivities at the MEMS-scale, but was limited in its ability to predict reactor dimensions as it could not account for the length required to vaporize the hydrogen peroxide, or the importance of inlet boundary condition on system performance.

In this study, the performance of the catalytic chamber pre-vaporization is evaluated. This study serves as a natural complement to the work performed by Widdis, Asante *et al.* (2013), as it investigates effects associated with the monopropellant in its liquid form. The impact of microscale effects on the decomposition of the liquid monopropellant is investigated in the general case of lamellar flow entering a catalytic bed, and compared with performance of the discrete propellant delivery system.

2. Computational methodology

To study the effect of liquid phase HTP entering the catalytic chamber, a computational model was developed to characterize the decomposition of hydrogen peroxide. The model tracks the species formation and heat generation associated with the decomposition. The model is allowed to run to 423 K, the vaporization temperature of hydrogen peroxide, at which point it terminates as phase change is not considered. This study necessarily involves the modeling of multiple physics; the decomposition of the hydrogen peroxide and the transport of chemical species by fluid flow must be modeled. Additionally, there are two flow regimes considered: lamellar flow and slug flow. The specific details of each model, and the methodology for linking them, are delineated below.

2.1 Governing equations

2.1.1 Chemical reaction

The chemical kinetic rate constant k and reaction rate r are modeled according to first-order Arrhenius kinetics

$$k = A \exp\left(\frac{-E_a}{RT}\right) \quad (1)$$

$$r = k C_{HTP} \quad (2)$$

where E_A is a catalyst-dependent activation energy, R is the universal gas constant, T is the temperature and C_{HTP} is the concentration of hydrogen peroxide. Zhou and Hitt (2005) calculated the activation energy of an effective catalyst as 52.5 kJ/mol, and this value has been used for these studies. The pre-exponential factor (A) has units of s^{-1} and acts as a scaling factor that varies with surface area to volume ratio. In a previous study, Zhou and Hitt (2005) estimated $A=10^9 s^{-1}$, which is consistent with value according to collision theory and has been used for these studies.

The transport equations for species is given by

$$-\frac{\partial c_i}{\partial t} + \mathbf{u} \cdot \nabla c_i = \nabla \cdot (D_i \nabla c_i) + R_i \quad (3)$$

where c_i is the concentration of the species of interest, \mathbf{u} is the velocity field, D_i is the mass diffusivity of the species of interest, and R_i is the source or sink of the species of interest. The transport equation for the energy is given by

$$\rho C_p \frac{\partial T}{\partial t} + \rho C_p \mathbf{u} \cdot \nabla T = \nabla \cdot (k \nabla T) + Q \quad (4)$$

where C_p is the specific heat, T is the temperature, and k is the thermal conductivity of the monopropellant, and Q is a heat flux term.

Initial material properties are determined from the bulk concentration on a molar average. The mass diffusivity of liquid hydrogen peroxide is taken as $4E-9 m^2/s$. It is worth noting that this value is much lower than the gas diffusivity of hydrogen peroxide, which will be explored in more detail in the Results section below.

In this model, the surface effects arising from the catalytic nanorods are ignored and instead regarded as a perfect surface coating. Given the scale of the nanostructures, this is likely a good approximation. If necessary, however, their impact could theoretically be accounted for by adjusting the pre-exponential factor to match experimental results.

The equations governing the velocity field (\mathbf{u}) are either the unsteady Navier-Stokes, or the multiphase, unsteady Navier-Stokes. Each of these sets of equations is described in the following section.

2.1.2 Laminar flow

The unsteady Navier-Stokes equations were solved to find the flow field within the computational domain. Due to the extremely low Re number ($\sim O[1]$), the flow is laminar at all points in the simulation. The momentum and continuity equations, respectively, are presented here

$$\rho \frac{\partial \mathbf{u}}{\partial t} + \rho (\mathbf{u} \cdot \nabla) \mathbf{u} = \nabla \cdot [-p \mathbf{I} + \mu (\nabla \mathbf{u} + (\nabla \mathbf{u})^T)] + \mathbf{F} \quad (5)$$

$$\nabla \cdot \mathbf{u} = 0 \quad (6)$$

where \mathbf{u} is the velocity field of the fluid, ρ is the fluid density, p is the pressure, μ is the dynamic viscosity and \mathbf{F} is the surface tension force.

The flow field is discretized using linear Lagrange elements for velocity and pressure field (P1+P1). It is directly solved using a PARDISO solver. The steady-state solution is obtained using

a pseudo time stepping procedure, and convergence of the solution is assessed via residuals.

2.1.3 Slug flow

The two-phase flow field is governed by the incompressible Navier-Stokes Equations

$$\rho_i \frac{\partial \mathbf{u}_i}{\partial t} + \rho_i (\mathbf{u}_i \cdot \nabla) \mathbf{u}_i = \nabla \cdot [-p\mathbf{I} + \mu_i (\nabla \mathbf{u}_i + (\nabla \mathbf{u}_i)^T)] + \mathbf{F} \quad (7)$$

$$\nabla \cdot \mathbf{u}_i = 0 \quad (8)$$

where the variables are the same as in Eqs. (5)-(6), but the subscript \mathbf{i} corresponds to the appropriate gas or liquid phase. To track the interface between the two phases, the level set method was used. In the level set method, the discontinuity between two discrete phases is represented with the level set function Φ , a continuous function bounded by zero and unity that represents the normalized distance from the interface at all points in the domain (Osher and Sethian 1998). As the flow field is calculated, the movement of the interface is calculated by

$$\frac{\partial \phi}{\partial t} + \mathbf{u} \cdot \nabla \phi = \phi(1 - \phi) \frac{\nabla \phi}{|\nabla \phi|} \quad (9)$$

The discontinuity in density and viscosity are smoothed across the interface using equations

$$\rho = \rho_1 + (\rho_2 - \rho_1)\phi \quad (10)$$

$$\nu = \nu_1 + (\nu_2 - \nu_1)\phi \quad (11)$$

The surface tension equation can then be recast in terms of the surface tension coefficient and the level set function

$$\mathbf{F}(x) = \sigma \kappa(x) \hat{\mathbf{n}}(x) \quad (12)$$

In this formulation, the surface tension represents a volume force that is spread across the width of the interface. The new force is only equal to the surface tension in the limit as the thickness of the interface goes to zero, which places an upper bound on the maximum width of the interface. If the interface gets too small, however, the discontinuity in density and viscosity cannot be properly smoothed, which yields difficulties in computing the solution. This puts boundaries on the grid refinement, which will be addressed below. For the slug flow simulations, a second order Lagrange element is used for velocity and linear Lagrange elements are used for pressure. This system is directly solved using a PARDISO solver, and convergence is assessed by monitoring the residuals.

2.1.4 Physics coupling

The chemical reaction and flow field are solved simultaneously, as many of the species transport and fluid thermophysical properties are temperature dependent. At each time step the release of energy from the decomposition is calculated and used to update the temperature of the fluid. This data then feeds into a coupled solver that updates the flow field based on the inlet conditions and the temperature information. Finally, these data are used to compute the species transport, which is used to compute the local decomposition rate. The solver runs until the temperature in the domain reaches 423 K, at which point it terminates.

2.2 Computational domain and boundary conditions

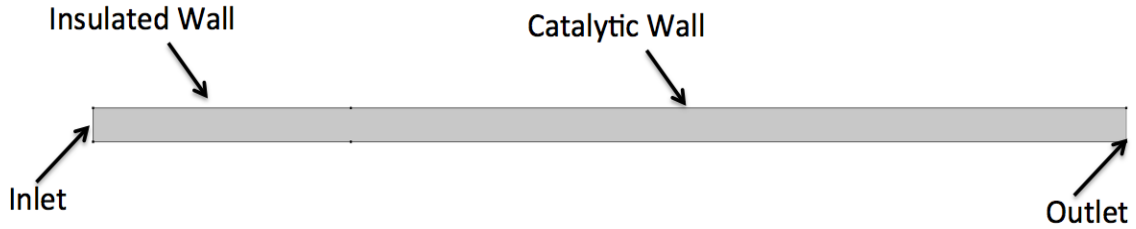


Fig. 4 Computational geometry of the straight microchannel

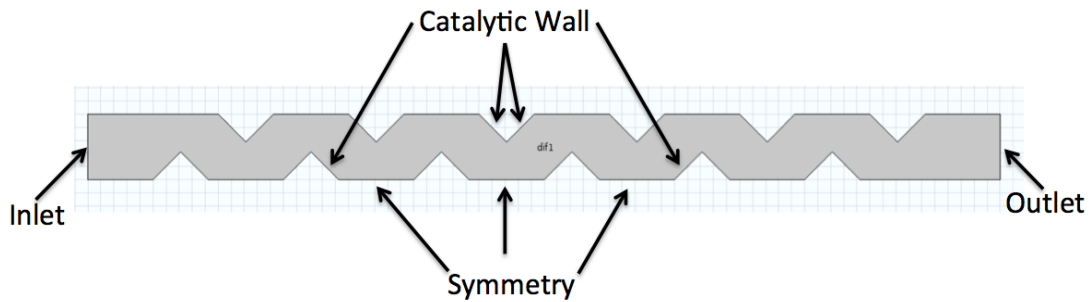


Fig. 5 Catalytic pillar computational domain

2.2.1 2D model of a catalytic wall

A slender straight channel was first modeled to apply the reaction kinetics to a fluid flow in order to determine system performance at mass flow rates consistent with the micropropulsion application. The length of the channel is $1600 \mu\text{m}$, which is consistent with the length of the catalyst bed in other MEMS-based microthrusters. The flow is assumed to be unidirectional and the geometry lacks all complexities of the pillar-based catalyst bed design. This geometry is shown in Fig. 4. The inlet is a laminar inflow condition, and has been set to a prescribed temperature of 293 K and a flow rate of 1.2 m/s . Species inflow is prescribed at 100% concentration of H_2O_2 . The walls in the first $200 \mu\text{m}$ of the channel have been set as an insulated wall, with the remainder acting as a catalytic surface. This has been done to prevent heat from being conducted upstream through the boundary. The outlet is a pressure outlet (1 atm). This is the only mode for heat to exit the system.

2.2.2 2D model of catalytic pillar geometry

For comparison with the straight channel geometry, a section of the pillar array was studied, as shown in Fig. 5. This section is intended to model flow through the middle of the pillar array, and uses symmetry along the top and bottom planes. The pillars are assumed to be evenly coated in the nanorods, and serve as the reaction sites. The inlet is a laminar inflow, while the outlet pressure condition is 1 atm .

2.2.3 2D model of a catalytic wall with slug flow

To study the effects of multiphase flow entering the catalytic chamber, the 2D slender channel was modified to provide the necessary conditions to generate slug flow. This can be accomplished

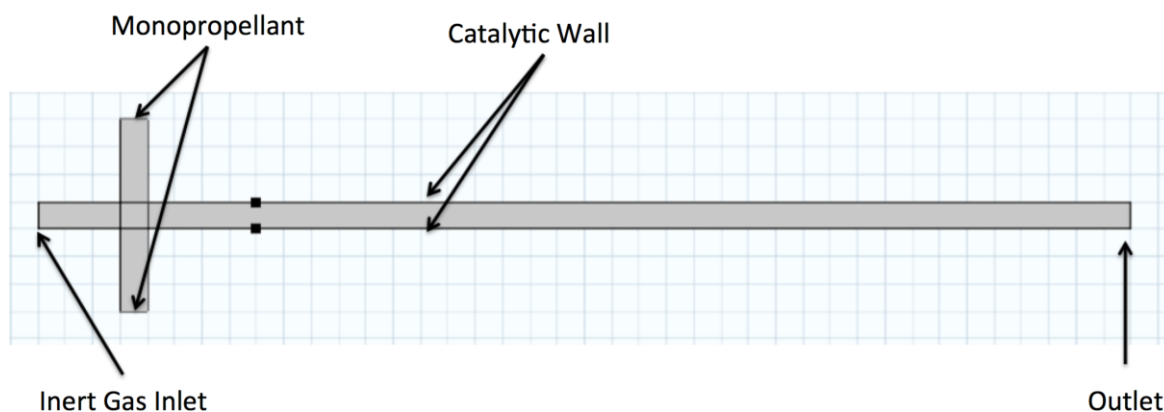


Fig. 6 Slug flow computational domain

at the microscale by having two immiscible fluids meeting at a cross-junction. In this model, two of the inlets are hydrogen peroxide, while the third inlet is air, with each inlet set to a flow rate of 0.4 m/s. The outlet is set at 1 atm. The wall after the junction is set as a reacting wall.

2.3 Grid generation and convergence

2.3.1 Lamellar flow

To model the lamellar flow regime, a structured mesh was generated for the computational domains presented previously. A systematic grid refinement study was performed to ensure that results are insensitive to further grid refinement. The result was a grid consisting of 33720 elements.

2.3.2 Multiphase flow

To accurately model multiphase flow, the grid must be smaller than the projected interface thickness at all locations that it may travel. To increase solution speed, adaptive mesh refinement was used. This method generates a coarse unstructured mesh within the computational domain. The number of elements is then increased in regions where there is a gradient of the level set function (i.e., at the interface between the two fluids). Convergence is achieved when the interface is resolved, as determined by the percent difference change in interface thickness. At successive time steps, this process is repeated to ensure that the mesh adapts to the changing topology of the interface. While this method precludes traditional grid convergence studies, the continuous refinement of the mesh is intended to keep it optimized.

To confirm that the results generated while using adaptive mesh refinement are comparable to a fixed mesh simulation, models were solved using each method. While there are qualitative differences between the two simulations, it is worth noting that the primary goal of this work is to characterize the performance in the catalytic chamber, which is necessarily going to involve the measurement of many slugs. Thus small variations in individual slugs are going to be less important than the average slug characteristics. For the model studied, the slugs in the model with adaptive mesh refinement were 2% larger than on a fixed mesh. As the processing time for a single simulation was an order of magnitude smaller (2 hours for adaptive mesh refinement vs. 20 hours

for fixed mesh) and this study would involve a number of simulations, adaptive mesh refinement was deemed to be acceptable.

3. Results

3.1 2D catalytic wall-laminar flow

A sample image of the concentration of hydrogen peroxide in the straight channel is shown in Fig. 8. In the computational domain, only the region of fluid in contact with the wall, or very nearby, is decomposed. This is because at the microscale, diffusion is the only mechanism transporting the hydrogen peroxide to the catalyst. The much lower mass diffusivity of liquid hydrogen peroxide than in its gaseous state, means that a reactor sized for optimal vapor phase performance will suffer from poor performance before vaporization occurs. The results observed in this model are similar to the straight channel experimental results presented in Widdis, Asante *et al.* (2013), shown in Fig. 7. In those experiments, incomplete decomposition of the hydrogen peroxide was observed in a straight microchannel with reactive walls. The authors of that paper theorized that the incomplete decomposition was related to the lack of a convective mixing mechanism, such as turbulence, combined with the relatively low mass diffusivity of hydrogen peroxide.

The results of this computational model support that experimental effort, as they show that the

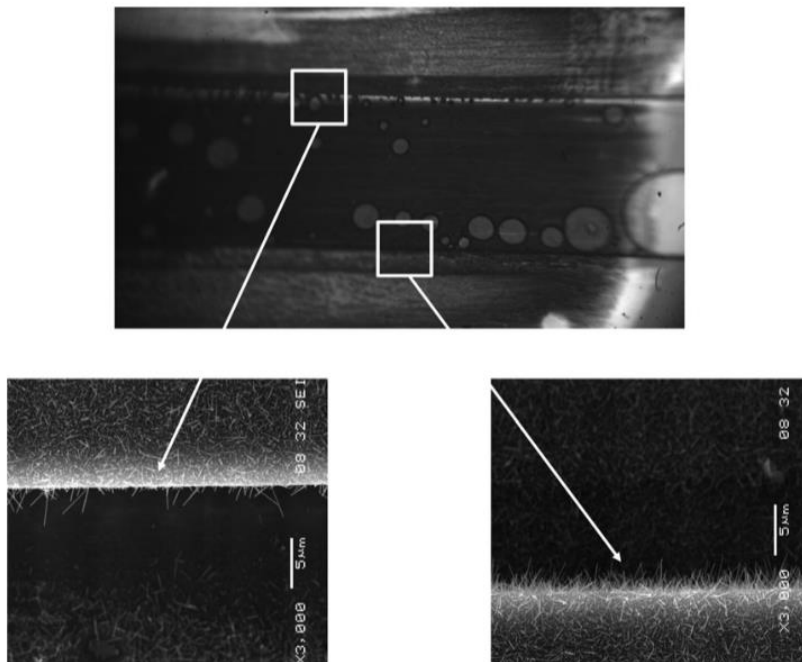


Fig. 7 Images depicting the straight channel catalytic wall previously studied. *Reproduced with permission from Widdis, Asante et al. (2013)*

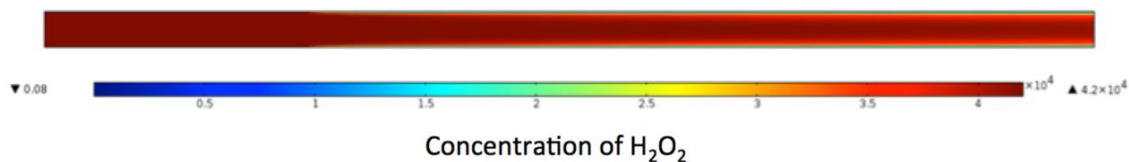


Fig. 8 Surface plot of hydrogen peroxide concentration in the straight channel (mol/m^3)

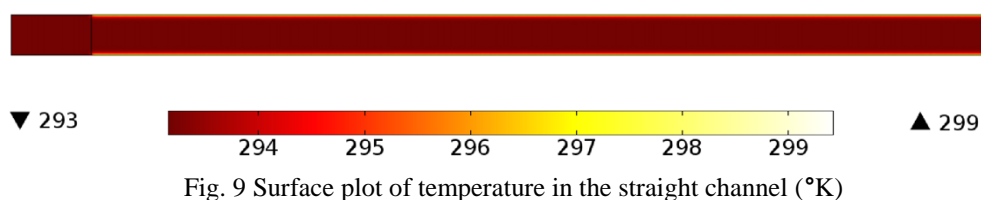


Fig. 9 Surface plot of temperature in the straight channel ($^{\circ}\text{K}$)



Fig. 10 Image of decomposition in a pillar array. *Reproduced with permission from Widdis, Asante et al. (2013)*

low mass diffusion in the liquid-phase make vaporization, and complete decomposition, challenging. Specifically, this can be seen in Fig. 8, where reaction has only occurred in a narrow region near the catalytic wall. The simulations indicate that this region of decomposed products act as a barrier to unreacted HTP coming in contact with the catalytic surface.

Fig. 9 shows the temperature profile of the channel; the heat generated by the decomposition has only raised the temperature by 6 degrees, well below the temperature required for sustainable decomposition. The heat generated along the reacting wall does not propagate into the bulk flow during the simulation.

3.2 2D pillar geometry

Having examined decomposition in the simplified catalytic wall model, the geometric impact of a pillar configuration was next considered. These studies were intended to model the behavior observed in Widdis, Asante *et al.* (2013), where decomposition was enhanced by flow the pillar array. The authors of that study theorized that this enhancement is due to the increase in surface area when compared to a straight channel of equal length. While greater decomposition was observed in the pillar array, as shown in Fig. 10, there was still incomplete decomposition over the length tested. This behavior was not predicted by previous chemical decomposition models that primarily focus on the gas-phase decomposition.

For these studies, the pillars are $40\ \mu\text{m}$ pillars with $20\ \mu\text{m}$ spacing. Representative results are shown in Fig. 11. The purpose of the nanorod-coated pillars is to enhance decomposition when

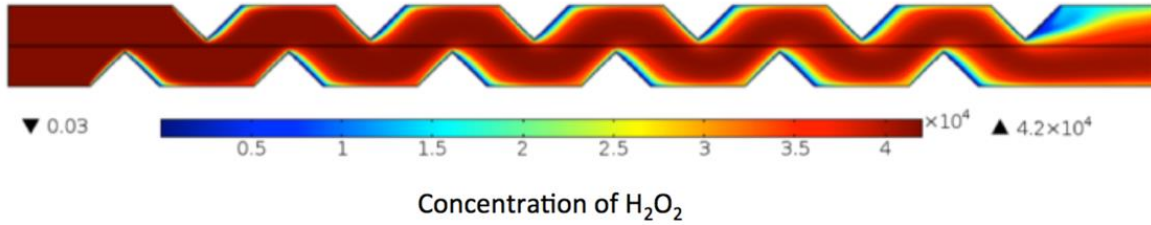
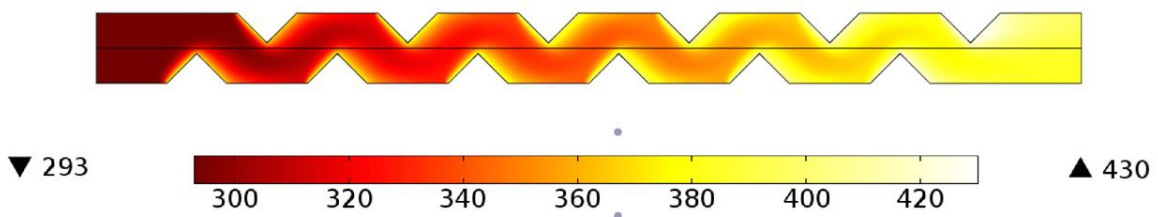
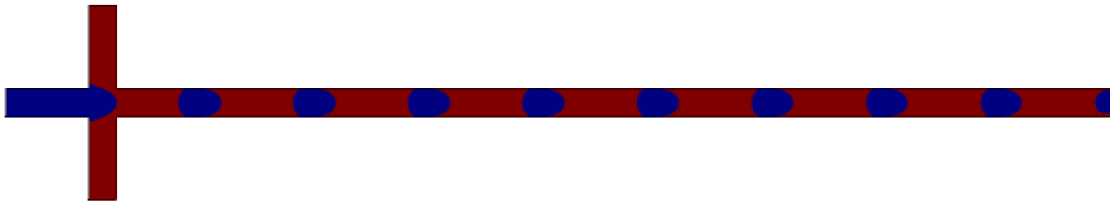
Fig. 11 Surface plot of hydrogen peroxide concentration in the pillar array (mol/m^3)Fig. 12 Surface plot of temperature in the pillar array ($^{\circ}\text{K}$)

Fig. 13 Surface plot of the slugs (in red) and bubbles (in blue) that result from the inlet conditions

compared to a straight channel. While differences in channel lengths make a direct comparison difficult, qualitatively, it can be observed that there are regions near the wall, where decomposition is much better than in the straight channel. The addition of the pillars serves to increase the reactive surface in contact with the flow for a given channel length. In a geometry that is nearly a quarter of the length, the average hydrogen peroxide concentration is slightly lower than the straight channel; presumably, over an equivalent domain length that performance would be improved even further. One challenge associated with the introduction of the pillars is the pressure drop associated with obstructing the flow. This sets an upper limit on the number of pillars that can be in the channel, if a desired mass flow rate is to be achieved. Therefore, for a given channel length, increasing the pillars can only be part of the solution for enhancing performance.

3.3 2D Catalytic wall-slug flow

In McDevitt and Hitt (2013), species transport in a microchannel was found to be enhanced in the slug flow regime. This enhancement is a result of the internal recirculation of the slugs that pulls the species from the center of the slug toward the exterior of the slug. While reviewing the poor performance exhibited by the catalytic chamber in these simulations, it was theorized that a

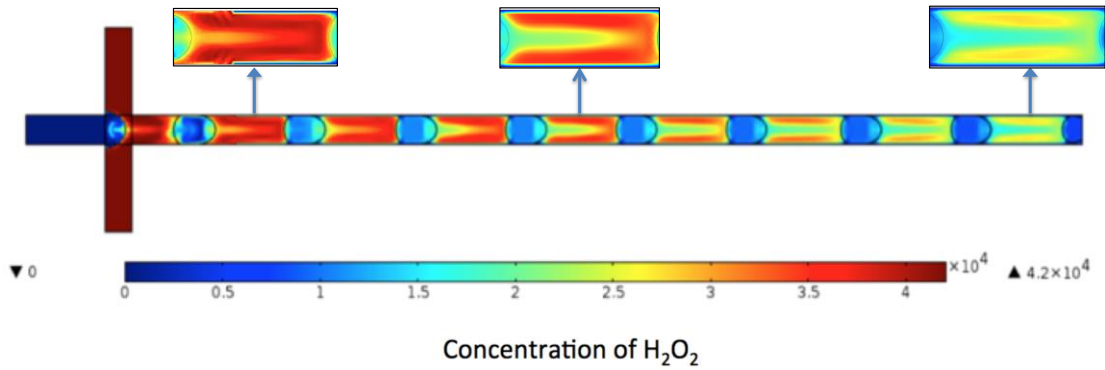


Fig. 14 Representative results of the decomposition in the microchannel with slug flow. The callouts highlight the enhancement offered by the internal recirculation of the slugs (mol/m^3)

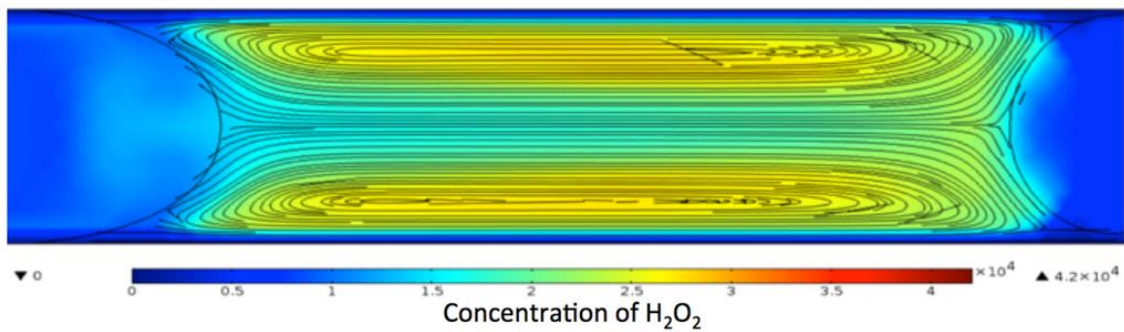


Fig. 15 Plot of the streamlines within the slug, emphasizing the internal recirculation that enhances decomposition (mol/m^3)

similar enhancement would be found in the heterogeneous catalytic chamber if slug flow were used instead of laminar flow. To orient the reader, Fig. 13 is a plot of slug flow in the computational domain, showing the slugs (in red) and bubbles (in blue).

Fig. 14 shows representative results of the simulations of hydrogen peroxide decomposition in the slug flow regime. When compared to the straight channel, the concentration of hydrogen peroxide at the outlet has decreased by over 36%. A thruster using slug flow could have a catalytic chamber that is less than half as long to achieve equivalent decomposition. As theorized, this enhancement comes from the internal recirculation within the slugs, which can be clearly seen in Fig. 15. As the slug moves down the channel, it pulls unreacted hydrogen peroxide from the center of the channel toward the wall, where it can come into contact with the catalyst. This mechanism is much more effective than diffusion, which accounts for the dramatically improved performance.

To characterize the improvement, the average concentration across the microchannel was calculated at several downstream locations for both the laminar and slug flow systems. The results of these calculations are plotted in Fig. 16. Beyond the absolute improvement in performance, it is worth noting that the rate of decomposition in the lamellar flow regime is lower than that of the slug flow regime. Presumably, over a longer domain this would result in a greater relative improvement for the slug flow system.

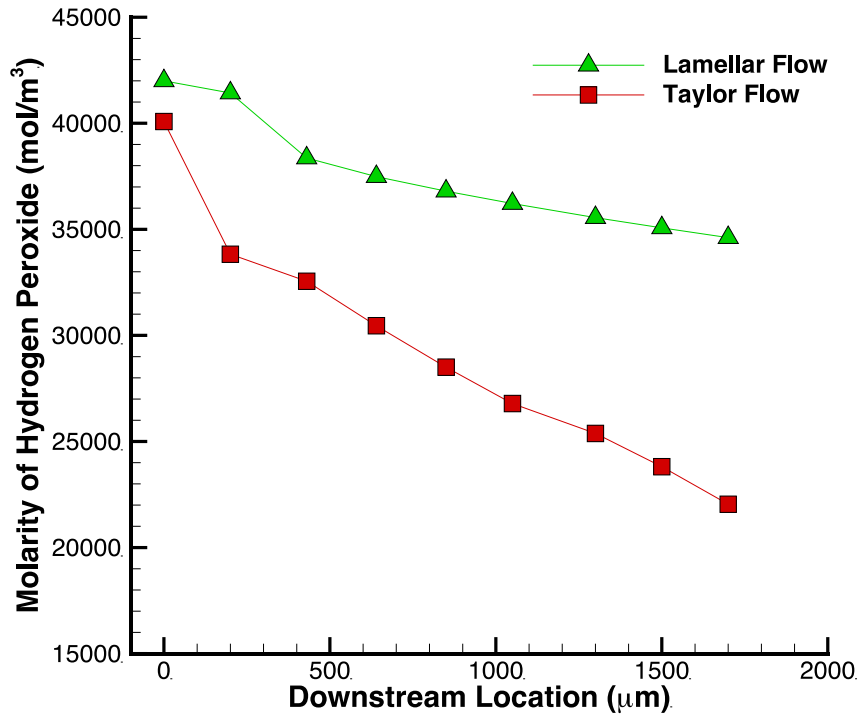


Fig. 16 Comparison of the average concentration at downstream locations in the slug flow and laminar flow systems

4. Discussion

A major consideration in the development of the catalytic chamber is the optimization of the chamber for both the entrance (liquid phase) and exit (gas phase). For purely laminar flow, a comparison of the Lewis numbers at the entrance ($\sim O[100]$) and exit ($\sim O[.01]$) demonstrate the relative importance of thermal diffusivity at the onset of decomposition and mass diffusivity at the completion. In the liquid phase, the significant decomposition mechanism is thermal diffusion; at the length scales considered for this study, this mechanism was insufficient for generating complete decomposition. Although not demonstrated in this study, it is a reasonable conclusion that a perfectly thermally insulated channel of sufficient length would allow the heat of decomposition to raise the bulk flow temperature sufficiently to allow for self-accelerating decomposition. In practice, however, some heat will be lost through the channel walls, and as such it may be challenging to create a microchannel long enough to raise the bulk flow temperature without losing too much heat. Combine that with the need to minimize dimensions for the proposed MEMS application, and it becomes clear that a decomposition mechanism that relies solely on thermal diffusivity faces several challenges. It is possible to pre-heat the hydrogen peroxide, to bring it closer to the vaporization temperature before decomposition begins. At the MEMS scale, this is typically done by placing a thermally resistive heater in the fuel injection system. For the intended micropropulsion application, this adds an additional power draw to a potentially power limited system.

As shown in this study, another method for overcoming the limitations of the thermal diffusivity decomposition mechanism is to generate a convective flow pattern within the channel using slug flow. The recirculation patterns within the slugs have the dual benefit of bringing high temperature HTP into the bulk flow and bringing unreacted HTP to the catalyst. Although the generation of slug flow requires an additional source of compressed gas, it has been demonstrated previously by the authors (McDevitt and Hitt 2012, 2013) that slug flow can also be used as a throttling mechanism to lower the minimum impulse-bit of a microthruster, an important consideration in nanosatellite attitude control. A microthruster developed to use the propellant throttling of slug flow will have the significant added benefit of enhanced decomposition.

5. Conclusions

In this study, a numerical model of hydrogen peroxide decomposition in a microreactor with a micropropulsion application was developed. This model builds upon the work of Widdis, Asante *et al.* (2013) by focusing on performance of the catalytic chamber before vaporization begins. This adds to the development of the model, as it provides information about the engineering challenges present before the hydrogen peroxide begins to vaporize.

The major findings of this work are twofold: at the microscale, the lack of a non-diffusive mixing mechanism inhibits the performance of the catalytic chamber, and that performance can be enhanced by forcing the flow regime into a slug flow pattern. The effect of mass diffusion in the vapor phase has been studied previously, by Widdis, Asante *et al.* (2013) and the findings here support those findings; in purely laminar flow, the low mass diffusivity of hydrogen peroxide leads to incomplete decomposition, or extremely long decomposition lengths that are not appropriate for the micropropulsion application.

The second finding is that for a given channel length, decomposition can be enhanced by improving mixing within the channel. In this study, the flow in a microchannel is forced into the slug flow regime through the addition of an immiscible gas. As these slugs flow down the microchannel, internal recirculation pulls unreacted flow from the center of the slug toward the reacting walls. This convective mixing mechanism is much more effective than diffusion, and results in a much higher rate of decomposition at equal channel lengths.

Acknowledgments

This work was supported by NASA under Cooperative Agreement #NNX09AO59.

References

- Cervone, A., Torre, L., d'Agostino, L., Musker, A., Roberts, G., Bramanti, C. and Saccocia, G. (2006), "Development of hydrogen peroxide monopropellant rockets", *Proceedings of the 42nd AIAA/ASME/SAE/ASEE Joint Propulsion Conference*, Sacramento, CA, July.
- Gauer, M., Telitschkin, D., Gotizg, U., Batonneau, Y., Johansson, H., Ivanov, M., Palmer, P. and Wiegerink, R. (2014), "First results of PRECISE-development of a MEMS-based monopropellant micro chemical propulsion system", *Acta Astronautica*, **93**, 77-83.
- Hitt, D.L., Zakrzewski, C. and Thomas, M. (2001), "MEMS-based satellite micropropulsion via catalyzed

- hydrogen peroxide decomposition”, *J. Smart Mater. Struct.*, **10**, 1163-1175.
- Huh, J. and Kwon, S. (2014), “Design, fabrication and thrust measurement of a micro liquid monopropellant thruster”, *J. Micromech. Microeng.*, **24**(10), 104001.
- Krejci, D., Woschnak, A., Scharlemann, C. and Ponweiser, K. (2012), “Structural impact of honeycomb catalysts on hydrogen peroxide decomposition for micro propulsion”, *Chem. Eng. Res. Des.*, **90**(12), 2302-2315.
- Krejci, D., Woschnak, M., Scharlemann, C., Ponweiser, K., Brahmi, R., Batonneau, Y. and Kappenstein, C. (2013), “Assessment of catalysts for hydrogen-peroxide-based thrusters in a flow reactor”, *J. Propuls. Power*, **29**(2), 321-330.
- Louisos, W.F. and Hitt, D.L. (2008), *Supersonic Micronozzles, Encyclopedia of Microfluidics and Nanofluidics*, Springer Publishing, New York, New York, USA.
- McDevitt, M. and Hitt, D. (2011), “Numerical study of disperse monopropellant slug formation at cross junction”, *Proceedings of the 41st AIAA Fluid Dynamics Conference*, Honolulu, HI, June.
- McDevitt, M. and Hitt, D. (2013), “Enhanced laminar mixing in multifluid droplets via multiphase flow in a microchannel”, *Proceedings of the 43rd AIAA Fluid Dynamics Conference*, San Diego, CA, June.
- Mueller, J., Hofer, R. and Ziemer, J. (2010), *Survey of Propulsion Technologies Applicable to CubeSats*, Jet Propulsion Laboratory, Pasadena, CA.
- NASA Mission Design Division Staff (2014), *Small Spacecraft Technology State of the Art*, Moffat Field, CA.
- Osher, S. and Sethian, J. (1988), “Fronts propagating with curvature-dependent speed: algorithms based on Hamilton-Jacobi formulations”, *J. Comp. Phys.*, **79**, 1249.
- Thomas, M.A. (2000), “Design and testing of hydrogen peroxide microelectricalmechanical system”, Ph.D. Dissertation; George Washington University, Washington D.C., USA.
- Valenzuela, J., Garcia, C., Garcia, Z. and Choudhurri, A. (2011), “HTP decomposition in millimeter scale channel type catalytic reactors”, *Proceedings of 47th AIAA/ASME/SAE/ASEE Joint Propulsion Conference and Exhibit*, San Diego, CA, July/August.
- Whitehead, J. (1998), “Hydrogen peroxide propulsion for smaller satellites”, *Proceedings of 1st International Hydrogen Peroxide Propulsion Conference*, Guildford, UK.
- Widdis, S., Asante, K., Hitt, D., Cross, M., Varhue, W. and McDevitt, M. (2013), “A MEMS-based catalytic micro-reactor for a H₂O₂ monopropellant micropropulsion system”, *IEEE/ASME Tran. Mech.*, **1**, 1-9.
- Zhou, X. and Hitt, D.L. (2003), “One-dimensional modeling of catalyzed H₂O₂ decomposition in microchannel flows”, *Proceedings of 33rd AIAA Fluid Dynamics Conference and Exhibit*, Orlando, FL, June.
- Zhou, X. and Hitt, D.L. (2004), “Modeling of catalyzed hydrogen peroxide decomposition in slender microchannels with arrhenius kinetics”, *Proceedings of 40th AIAA/SAE/ASEE Joint Propulsion Conference and Exhibit*, Ft. Lauderdale, FL, July.
- Zhou, X. and Hitt, D.L. (2005), “Numerical modeling of monopropellant decomposition in a micro-catalyst bed”, *Proceedings of 35th AIAA Fluid Dynamics Conference and Exhibit*, Toronto, Canada, June.